# Probing New Bosons and Nuclear Structure with Ytterbium Isotope Shifts

Menno Door,[1,2,*,†] Chih-Han Yeh,[3,*,‡] Matthias Heinz,[4,5,1,§] Fiona Kirk,[3,6] Chunhai Lyu,[1] Takayuki Miyagi,[4,5,1] Julian C. Berengut,[7] Jacek Bieroń,[8] Klaus Blaum,[1] Laura S. Dreissen,[3,9] Sergey Eliseev,[1] Pavel Filianin,[1] Melina Filzinger,[3] Elina Fuchs,[3,6] Henning A. Fürst,[3,10] Gediminas Gaigalas,[11] Zoltán Harman,[1] Jost Herkenhoff,[1] Nils Huntemann,[3] Christoph H. Keitel,[1] Kathrin Kromer,[1] Daniel Lange,[1,2] Alexander Rischka,[1] Christoph Schweiger,[1] Achim Schwenk,[4,5,1] Noritaka Shimizu,[12] and Tanja E. Mehlstäubler[3,10,13]

[1]*Max-Planck-Institut für Kernphysik, Saupfercheckweg 1, 69117 Heidelberg, Germany*
[2]*Heidelberg University, Grabengasse 1, 69117 Heidelberg, Germany*
[3]*Physikalisch-Technische Bundesanstalt, Bundesallee 100, 38116 Braunschweig, Germany*
[4]*Department of Physics, Technische Universität Darmstadt, Darmstadt, 64289, Germany*
[5]*ExtreMe Matter Institute EMMI, GSI Helmholtzzentrum für Schwerionenforschung GmbH, Darmstadt, 64291, Germany*
[6]*Institut für Theoretische Physik, Leibniz Universität Hannover, Appelstraße 2, 30167 Hannover, Germany*
[7]*School of Physics, University of New South Wales, Sydney, New South Wales 2052, Australia*
[8]*Institute of Theoretical Physics, Jagiellonian University, Kraków, 30-348, Poland*
[9]*Department of Physics and Astronomy, LaserLab, Vrije Universiteit Amsterdam, De Boelelaan 1081, Amsterdam, 1081 HV, The Netherlands*
[10]*Institut für Quantenoptik, Leibniz Universität Hannover, Welfengarten 1, 30167 Hannover, Germany*
[11]*Institute of Theoretical Physics and Astronomy, Vilnius University, Vilnius, 10222, Lithuania*
[12]*Center for Computational Sciences, University of Tsukuba, Ibaraki, 305-8577, Japan*
[13]*Laboratorium für Nano- und Quantenengineering, Leibniz Universität Hannover, Schneiderberg 39, 30167 Hannover, Germany*

(Received 23 June 2024; revised 6 November 2024; accepted 23 December 2024; published 11 February 2025)

In this Letter, we present mass-ratio measurements on highly charged $Yb^{42+}$ ions with a precision of $4 \times 10^{-12}$ and isotope-shift measurements on $Yb^+$ on the $^2S_{1/2} \rightarrow {}^2D_{5/2}$ and $^2S_{1/2} \rightarrow {}^2F_{7/2}$ transitions with a precision of $4 \times 10^{-9}$ for the isotopes $^{168,170,172,174,176}$Yb. We present a new method that allows us to extract higher-order changes in the nuclear charge distribution along the Yb isotope chain, benchmarking *ab initio* nuclear structure calculations. Additionally, we perform a King plot analysis to set bounds on a fifth force in the keV/$c^2$ to MeV/$c^2$ range coupling to electrons and neutrons.

DOI: 10.1103/PhysRevLett.134.063002

Theories beyond the standard model (SM) of particle physics are typically probed by high-energy colliders or astrophysical and cosmological observations. Competitive complementary tests can be performed with high-precision atomic and molecular physics experiments at low energies [1]. In particular, isotope-shift spectroscopy, commonly used to study nuclear charge radii in exotic isotopes [2], is also sensitive to shifts in atomic energy levels induced by hypothetical new bosons that mediate an additional interaction between neutrons and electrons [3,4]. Such measurements can be analyzed via the King-plot method, where different atomic transitions are combined in such a way that common nuclear and atomic uncertainties are eliminated. Deviations from the linearity of the King plot indicate effects from new physics or higher-order atomic and nuclear structure. This powerful technique has been successfully used to put bounds on physics beyond the SM, for example, with isotope shifts measured in ytterbium [5–7]. With increasing precision of the frequency measurements, the uncertainties of the nuclear masses [5,8] become a limiting factor for distinguishing between higher-order SM effects and new physics.

In this Letter, we present high-precision mass-ratio and isotope-shift measurements of five stable, spinless ytterbium isotopes. Both the mass spectrometry and the isotope-shift spectroscopy are up to 2 orders of magnitude more precise than previous measurements [7–9]. The isotope mass ratios are determined using highly charged Yb ions in the Penning-trap mass spectrometer Pentatrap [10], reaching

*These authors contributed equally to this work.
†Contact author: menno.door@lkb.upmc.fr
‡Contact author: chih-han.yeh@ptb.de
§Present address: National Center for Computational Sciences, Oak Ridge National Laboratory, Oak Ridge, Tennessee 37831, USA

a relative precision of a few $10^{-12}$ contributing to a relative uncertainty of $10^{-10}$ for the mass-normalized isotope shifts. The isotope-shift spectroscopy is performed on $Yb^+$ on the $^2S_{1/2} \rightarrow {}^2D_{5/2}$ and the $^2S_{1/2} \rightarrow {}^2F_{7/2}$ transitions with a relative precision as low as $10^{-9}$. Our results deviate significantly from some former mass-ratio and isotope-shift measurements. Using our improved data, we construct a generalized King plot [11] and extract a competitive spectroscopic exclusion bound on the coupling strength of potential new bosons to electrons and neutrons.

Combining these precise measurements with atomic structure calculations allows us to investigate higher-order nuclear structure effects in Yb isotopes [6] and extract changes in the quartic charge radius $\delta\langle r^4\rangle$ along the isotopic chain, providing a new window into nuclear deformation. Building on advances in *ab initio* nuclear structure calculations [12–15], we provide a first microscopic description of Yb nuclei starting from chiral effective field theory interactions [16] based on quantum chromodynamics. This method can provide direct insights into the evolution of nuclear charge distributions along isotopic chains towards exotic, neutron-rich nuclei.

*Theoretical framework*—An isotope shift is the difference in the frequencies of a given atomic transition in two different isotopes of the same element. Here, we consider the $^2S_{1/2} \rightarrow {}^2D_{5/2}$ electric quadrupole and the highly forbidden $^2S_{1/2} \rightarrow {}^2F_{7/2}$ electric octupole transitions, denoted as $\alpha$ and $\gamma$, in singly charged $Yb^+$ ions. We consider five stable, even Yb isotopes with mass numbers $A \in \{168, 170, 172, 174, 176\}$ containing four neighboring isotope pairs $(A, A')$ with $A' = A + 2$. The corresponding isotope shifts $\nu_\alpha^{A,A'} = \nu_\alpha^A - \nu_\alpha^{A'}$ make up the entries of a four-component vector $\boldsymbol{\nu}_\alpha$ for transition $\alpha$ (and similarly for $\gamma$). This vector $\boldsymbol{\nu}_\alpha$ can be written as a linear combination of the field and mass shifts [17], additional higher-order SM-based shifts, and a term induced by the interaction with the proposed boson. Each of these terms can be decomposed into an electronic factor (with subscript $\alpha$) and a vector encoding the nuclear structure:

$$\boldsymbol{\nu}_\alpha = F_\alpha \boldsymbol{\delta}\langle r^2\rangle + K_\alpha \boldsymbol{w} + G_\alpha^{(2)} \boldsymbol{\delta}\langle r^2\rangle^2 + G_\alpha^{(4)} \boldsymbol{\delta}\langle r^4\rangle + \frac{\alpha_{\mathrm{NP}}}{\alpha_{\mathrm{EM}}} D_\alpha \boldsymbol{h} + \ldots. \quad (1)$$

$F$, $K$, $G^{(2)}$, $G^{(4)}$, and $D$ are transition-dependent factors for the multiplicative electronic contribution to the field shift, mass shift, quadratic field shift, quartic shift, and a shift induced by a new boson, respectively. The components of $\boldsymbol{w}$ are $w^{A,A'} = m_{172}/m_A - m_{172}/m_{A'} = 1/\eta_A - 1/\eta_{A'}$, the inverse nuclear mass differences of the isotopes $A$ and $A'$ with respect to the nuclear mass of $^{172}$Yb. $\boldsymbol{\delta}\langle r^n\rangle$ is the four-vector with elements $\delta\langle r^n\rangle^{A,A'} = \langle r^n\rangle^A - \langle r^n\rangle^{A'}$, the differences between the $n$th moments of the nuclear charge distributions. $\boldsymbol{\delta}\langle r^2\rangle^2$ has the components $(\delta\langle r^2\rangle^2)^{A,A'} = (\delta\langle r^2\rangle^{A,176})^2 - (\delta\langle r^2\rangle^{A',176})^2$ constructed from squared radius differences. Additional higher-order SM contributions may also contribute to Eq. (1) at a given experimental accuracy. $\alpha_{\mathrm{NP}} = (-1)^{s+1} y_n y_e/(4\pi\hbar c)$ is the product of the coupling constants $y_n$ and $y_e$ of the new boson (with mass $m_\phi$ and spin $s$) to the neutron and electron. It enters the Yukawa potential $V_{\mathrm{ne}}(r) = \hbar c \cdot \alpha_{\mathrm{NP}} \cdot \exp(-r m_\phi c/\hbar)/r$ [4] generated by the new boson. We normalize $\alpha_{\mathrm{NP}}$ by the fine-structure constant $\alpha_{\mathrm{EM}} = e^2/(4\pi\hbar c)$, where $e$ is the elementary charge. $\boldsymbol{h} = -(2, 2, 2, 2)$ is the vector of neutron number differences for the neighboring isotope pairs.

Usually, only the first two terms in Eq. (1) contribute significantly. With isotope-shift measurements for two transitions $\alpha$ and $\gamma$, one can eliminate $\boldsymbol{\delta}\langle r^2\rangle$ from Eq. (1) so that the first two terms yield the linear King relation [4,17]

$$\tilde{\boldsymbol{\nu}}_\gamma \approx F_{\gamma\alpha} \tilde{\boldsymbol{\nu}}_\alpha + K_{\gamma\alpha} \mathbf{1}, \quad (2)$$

with the mass-normalized $\tilde{\boldsymbol{\nu}}_\gamma = \boldsymbol{\nu}_\gamma/\boldsymbol{w}$, $\mathbf{1} = (1, 1, 1, 1)$, $F_{\gamma\alpha} = F_\gamma/F_\alpha$, and $K_{\gamma\alpha} = K_\gamma - F_{\gamma\alpha} K_\alpha$. Deviations from Eq. (2) indicate the presence of additional terms beyond the leading-order field and mass shifts, as in Eq. (1).

*Experimental results*—The nuclear mass ratios $\eta_A$ of ytterbium isotopes are determined from the cyclotron frequency ratios of highly charged $Yb^{42+}$ ions measured at the cryogenic Penning-trap mass spectrometer Pentatrap [10,18,19] and their calculated electron binding energies. The determination of the cyclotron frequencies $\nu_c$ of two isotope ions allows one to extract their ionic mass ratio via $\mathrm{R}_A^{\mathrm{CF}} = \nu_c(^{172}\mathrm{Yb}^{42+})/\nu_c(^A\mathrm{Yb}^{42+}) = m(^A\mathrm{Yb}^{42+})/m(^{172}\mathrm{Yb}^{42+})$. Determining the free cyclotron frequency $\nu$ requires measuring all three eigenfrequencies of the trapped ion via $\nu_c^2 = \nu_+^2 + \nu_z^2 + \nu_-^2$ [20], namely, the trap-modified cyclotron frequency $\nu_+$, the axial frequency $\nu_z$, and the magnetron frequency $\nu_-$.

From the calculated electron binding energies $E_{172}^{(28)} = 350\,773(5)$ eV of the 28 electrons in the $^{172}Yb^{42+}$ ion and $E_{172}^{(70)} = 382\,301(16)$ eV of the 70 electrons in the $^{172}$Yb atom [21], the neutral mass $m(^{172}\mathrm{Yb})$ [9,22], and the electron mass $m_e$ [23], one can derive the necessary nuclear mass ratios $\eta_A$ to similar accuracies. The mass ratios are used instead of single mass values in atomic mass units, since the former are much less sensitive to the uncertainties of the binding energies and the reference mass $m(^{172}\mathrm{Yb})$. Their final values are given in Table I with relative uncertainties of $4 \times 10^{-12}$, corresponding to uncertainties of 0.3 Hz on the isotope shifts. For comparison, previous mass determinations affected the King-plot analysis at a level of 3–30 Hz.

To make use of the new mass uncertainties, we improve the uncertainties of the isotope shifts by performing absolute frequency measurements of the $\alpha$ and $\gamma$ transitions for the five isotopes. Singly charged ytterbium ions are trapped in a segmented, linear radio-frequency Paul trap [24,25]. The excitation lasers near wavelengths of 411 and

TABLE I. Measured values of the mass ratios and isotope shifts. Columns 2 and 3 show the $Yb^{42+}$ cyclotron frequency ratios and nuclear mass ratios of the stable, even ytterbium isotopes relative to the nuclear mass of isotope $A = 172$, with the differences to Refs. [8,9] given in Column 4. Columns 5 and 7 show the isotope shifts $\nu^{A,A+2} = \nu^{A} - \nu^{A+2}$ of the $\alpha$ transition and the $\gamma$ transition in units of Hz, with the differences to Ref. [5] for $\alpha$ given in Column 6. Our isotope shifts for the $\gamma$ transition are compatible with those of Ref. [7].

| $A$ | $R_A^{CF} = \nu_{c,172}/\nu_{c,A}$ | $\eta_A = m_A/m_{172}$ | $\Delta\eta_A$ $(10^{-12})$ | $\nu_{\alpha_{PTB}}^{A,A+2}$ (Hz) | $\Delta\nu_{\alpha}^{A,A+2}$ (Hz) | $\nu_{\gamma_{PTB}}^{A,A+2}$ (Hz) |
|---|---|---|---|---|---|---|
| 168 | 0.976 717 951 145(4) | 0.976 715 921 749(4) | −1890(780) [8] | 2179098868.0(5.3) | −62(210) [5] | −4438159671.1(15.7) |
| 170 | 0.988 356 814 144(4) | 0.988 355 799 258(4) | −88(108) [9] | 2044851281.0(4.9) | −3499(340) [5] | −4149190501.1(15.7) |
| 172 | ⋯ | ⋯ | ⋯ | 1583064149.3(4.8) | −4271(360) [5] | −3132320458.1(15.7) |
| 174 | 1.011 648 196 817(4) | 1.011 649 212 140(4) | 153(122) [9] | 1509053195.8(4.7) | −2094(280) [5] | −2976392045.3(15.7) |
| 176 | 1.023 303 526 697(4) | 1.023 305 557 965(4) | 68(173) [9] | ⋯ | ⋯ | ⋯ |

467 nm are locked to ultra-low-expansion cavities and to a cryogenic silicon cavity [26] via a frequency comb.

The absolute transition frequencies are obtained with optical frequency ratio measurements by referencing to the $\gamma$ transition between the $F = 0$ and $F = 3$ hyperfine states of the $^{171}Yb^{+}$ isotope [27]. From the measurements, we obtain isotope shifts shown in Table I, with uncertainties below 6 and 16 Hz for the $\alpha$ and the $\gamma$ transitions, respectively.

For details on the mass-ratio measurements, spectroscopic measurements, systematic shifts, and uncertainties, see the End Matter and Supplemental Material [28].

*King-plot analysis*—A King plot using our mass-normalized isotope-shift measurements of the $\gamma$ transition (denoted $\tilde{\nu}_{\gamma_{PTB}}$) and the $\alpha$ transition (denoted $\tilde{\nu}_{\alpha_{PTB}}$) is given in the End Matter. From the King-plot analysis, we observe deviations from linearity averaging to 20.17(2) kHz.

To determine the origin of the nonlinearity in the King plot, we perform a nonlinearity decomposition analysis of all available (sub-)kHz-precision isotope-shift data. Apart from $\alpha_{PTB}$ and $\gamma_{PTB}$ presented in this Letter these are $\alpha_{MIT}$ and $\gamma_{MIT}$ from Ref. [7], the $^2S_{1/2} \rightarrow {}^2D_{3/2}$ transition in $Yb^{+}$ [5] (denoted $\beta$), $^1S_0 \rightarrow {}^3P_0$ in Yb [80] (denoted $\delta$), and $^1S_0 \rightarrow {}^1D_2$ in Yb [81] (denoted $\epsilon$). In total, we construct 7 mass-normalized isotope-shift vectors $\tilde{\boldsymbol{\nu}}_\tau$, with $\tau \in \{\alpha_{PTB}, \alpha_{MIT}, \beta, \gamma_{PTB}, \gamma_{MIT}, \delta, \epsilon\}$. Since these vectors are four vectors, they are uniquely described by their projections onto four basis vectors. We choose the basis vectors $\tilde{\boldsymbol{\nu}}_\delta$ and $\mathbf{1}$, which span the plane of King linearity [see Eq. (2), with $\alpha \rightarrow \delta$], and $\boldsymbol{\Lambda}_+$ and $\boldsymbol{\Lambda}_-$ (defined in Supplemental Material [28]), which are orthogonal to this plane [7]. We obtain $\tilde{\boldsymbol{\nu}}_\tau = F_{\tau\delta}\tilde{\boldsymbol{\nu}}_\delta + K_{\tau\delta}\mathbf{1} + \lambda_+^{(\tau)}\boldsymbol{\Lambda}_+ + \lambda_-^{(\tau)}\boldsymbol{\Lambda}_-$ with $F_{\tau\delta}$ and $K_{\tau\delta}$ as given in Eq. (2) and the coordinates $(\lambda_+^{(\tau)}, \lambda_-^{(\tau)})$ characterizing the deviation of the isotope shift $\boldsymbol{\nu}_\tau$ from the linear relation in Eq. (2). As shown in Fig. 1(a), the data points $(\lambda_+^{(\tau)}, \lambda_-^{(\tau)})$ lie to a good approximation on the solid black line through the origin of the $(\lambda_+, \lambda_-)$ plane. This implies that the tension of the Yb isotope-shift data with respect to King linearity can to a large extent be explained by a nonlinearity source (new physics, for example) with the appropriate slope $\lambda_-/\lambda_+$ in the decomposition plot. We compare the slope of the linear fit to the slopes predicted by the new physics term (dash-dotted line) and the quadratic field shift $\delta\langle r^2\rangle^2$ (dotted line, from experimental $\delta\langle r^2\rangle$ data [82]). Both have uncertainties not visible in Fig. 1(a), so we conclude that neither can be the leading source of the nonlinearity in the Yb King plot. Details of the nonlinearity decomposition are provided in the Supplemental Material [28] Another candidate is nuclear deformation [6,7], in particular $\delta\langle r^4\rangle$, which we predict using an *ab initio* approach.

*Nuclear structure effects*—Recent developments have made heavy nuclei accessible to *ab initio* nuclear structure calculations [15,83]. To predict $\delta\langle r^4\rangle$, we use the valence space in-medium similarity renormalization group (VS-IMSRG) [12,13] together with the quasiparticle vacua shell model (QVSM) [83] to solve the many-body Schrödinger equation. We employ nucleon-nucleon and three-nucleon interactions from chiral effective field theory, using the so-called 1.8/2.0 (EM) [84] and $\Delta N^2LO_{GO}$ [85] interactions, which differ in their construction and how they are fit to data, to give insight into interaction uncertainties. To assess many-body uncertainties, we solve the VS-IMSRG at the two- and three-body truncations [86] and employ two different valence spaces, VS1 with a $^{132}Sn$ core and VS2 with a $^{154}Gd$ core, in the QVSM. In Fig. 1(a), we show the prediction of the nonlinearity from our nuclear structure calculations, where the uncertainty is represented by the gray band. This uncertainty stems from a correlated statistical model accounting for interaction and many-body uncertainties including correlations between isotope pairs. Details of our nuclear structure calculations and the uncertainty quantification are provided in the Supplemental Material [28]. The two sets of calculations using the 1.8/2.0 (EM) Hamiltonian with valence spaces VS1 and VS2 serve as representative samples of our nuclear theory predictions. Since the best-fit line is compatible with the *ab initio* calculations for $\delta\langle r^4\rangle$, we assume $\delta\langle r^4\rangle$ to be the leading King-plot nonlinearity in Yb.

Combining isotope-shift measurements, nuclear mass-ratio measurements, and charge radius measurements [82] with atomic structure calculations of $G_\alpha^{(4)}$ [see Eq. (1)]

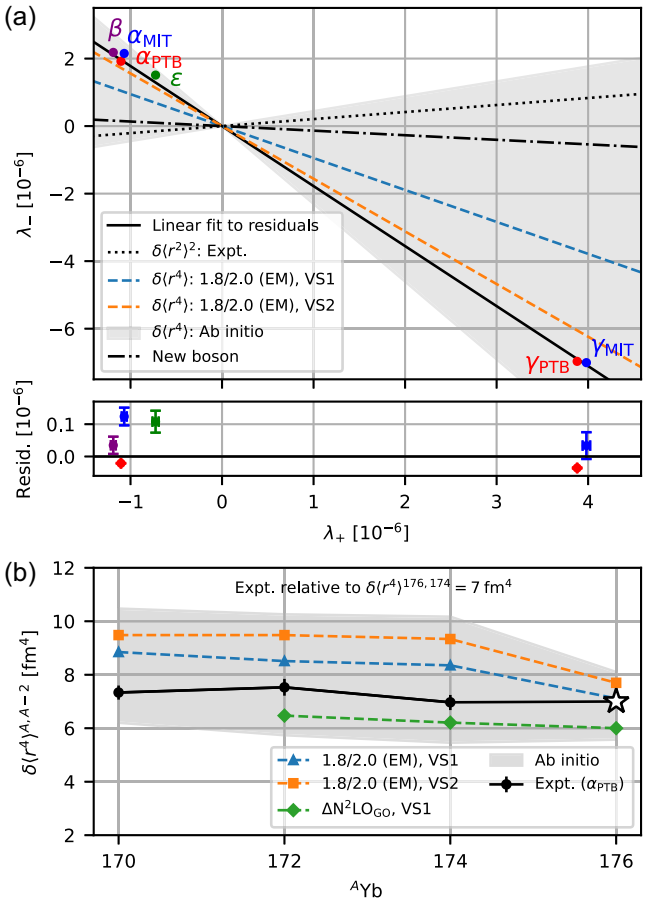


FIG. 1. Nonlinearity decomposition and the extracted trend of nuclear deformation, $\delta\langle r^4\rangle$. (a) Observed and predicted nonlinearities in the $(\lambda_+, \lambda_-)$ plane. The nonlinearities of the transitions $\alpha_{\mathrm{PTB}}$ (this Letter, see Table I), $\beta$ [5], $\gamma_{\mathrm{PTB}}$ (this Letter, see Table I), $\gamma_{\mathrm{MIT}}$ [5,7], and $\epsilon$ [81] with respect to the $\delta$ [80] transition are included in the single-source linear fit (solid line) whose slope is compared to the predicted slopes for the $\delta\langle r^2\rangle^2$ (dotted), $\delta\langle r^4\rangle$ [dashed lines and gray band based on predictions in (b)], and new physics (dash-dotted) nonlinearities. The residuals of the single-source linear fit are shown in the lower panel. (b) Solid line: $\delta\langle r^4\rangle^{A,A-2}$ values relative to $\delta\langle r^4\rangle^{176,174} = 7$ fm$^4$ (star) extracted from isotope shifts of the $\alpha_{\mathrm{PTB}}$ transition using atomic theory. Dashed lines: *ab initio* nuclear theory predictions [1.8/2.0 (EM), VS1 and VS2; $\Delta\mathrm{N^2LO_{GO}}$, VS1]. The estimated nuclear theory uncertainties (68% confidence interval) are given by the gray bands.

using AMBiT [87], we recast the Yb King-plot analysis into a measurement of nuclear deformation, which can be used to benchmark nuclear structure calculations. The procedure is given in the Supplemental Material [28], and the extracted changes in $\delta\langle r^4\rangle$ relative to the reference value of $\delta\langle r^4\rangle^{176,174} = 7$ fm$^4$ (star) are shown in Fig. 1(b). This reference value is based on input from both our *ab initio* results and density functional theory calculations [7] that all predict $\delta\langle r^4\rangle^{176,174} = 6$–$8$ fm$^4$. The experimental data show that the evolution of $\delta\langle r^4\rangle^{A,A-2}$ along the isotope chain is nearly flat, remarkably consistent with our *ab initio* calculations within uncertainties. Nonetheless, from the residuals for the transitions $\alpha_{\mathrm{PTB}}$, $\beta$, $\gamma_{\mathrm{PTB}}$, $\gamma_{\mathrm{MIT}}$, and $\epsilon$, shown in Fig. 1(a), we deduce a $23\sigma$ preference for more than one linearity, leaving open the possibility of a new boson being responsible for the next-to-leading King nonlinearity. This strengthens the prior two-source hypothesis [7] by a factor of more than 5.

*Bounds on new physics*—To extract bounds on the hypothetical new boson, we combine our isotope-shift measurements and nuclear mass measurements with the isotope-shift measurements of Ref. [80]. This allows us to eliminate both the charge radius variance $\delta\langle r^2\rangle$ and $\delta\langle r^4\rangle$ from the system of isotope-shift equations without requiring theoretical input. Assuming higher-order SM terms beyond $\delta\langle r^4\rangle$ to be negligible, the generalized King plot [11] can be used to set an upper bound on the new physics coupling $\alpha_{\mathrm{NP}}$ as a function of the mass $m_\phi$ of the new boson. Note that King-plot bounds should always be understood in the context of a given dataset since they are highly sensitive, not only to the central values and uncertainties of the frequency and mass measurements, but also to the unknown nuclear and electronic effects that are reflected in the isotope shift data. These aspects are discussed in more detail in the Supplemental Material [28].

The new bound provided by this Letter is shown in Fig. 2 in red. If the second King-plot nonlinearity were to be explained by new physics only, the couplings of the new boson would be expected to reside between the $2\sigma$ upper bound (solid red line) and the $2\sigma$ lower bound (dotted red line), which are only distinguishable in the inset. The new bound supersedes, both in precision and in magnitude, the $Ca^+$ King plot bounds [88,89] and the generalized King plot bounds using previous isotope shift data in $Yb^+$ [5,7,80] in combination with the new mass-ratio measurements provided by this Letter (see Table I). Moreover, it takes into account the significant shifts in the mass-ratio measurements $\eta_A$ and the isotope shifts $\nu_\alpha^{A,A+2}$ highlighted in Table I. For instance, the differences in the $\nu_\alpha^{A,A+2}$ measurements entering the bound from the dataset $(\alpha_{\mathrm{MIT}}, \gamma_{\mathrm{MIT}}, \delta)$ (shown in black) and the new bound (red) lead to the displacement of the characteristic peaks at the high end of the plotted $m_\phi$ values, resulting in different slopes. A detailed comparison of our new bound with respect to the bounds presented in Refs. [5,7], alongside a discussion of the competing astrophysical and laboratory bounds, which are shown in Fig. 2 as exclusion regions and green dashed curves, can be found in the Supplemental Material [28].

*Discussion and conclusion*—We measured the isotope shifts for the $^2S_{1/2} \rightarrow {}^2D_{5/2}$ electric quadrupole transition and the $^2S_{1/2} \rightarrow {}^2F_{7/2}$ electric octupole transition on five stable, spinless $Yb^+$ isotopes and with relative uncertainties on the order of $10^{-8}$ to $10^{-9}$, as well as mass ratios of these isotopes to a precision of $4 \times 10^{-12}$.

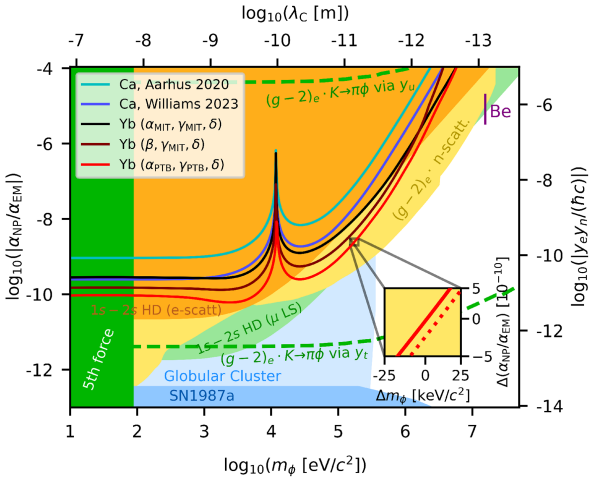


FIG. 2. Exclusion plot for the new boson $\phi$ coupling to electrons and neutrons. Solid lines: $2\sigma$ upper bounds from $Ca^+$ King plots (cyan: Aarhus [88], blue: Williams [89]), Yb$(^+)$ King plots (black, maroon: [5,7,80]), and from this Letter (red) on the product of couplings $y_e y_n/(\hbar c) = 4\pi\alpha_{\mathrm{NP}}$ to electrons and neutrons depending on the new boson's mass $m_\phi$. The inset shows an extract of the $2\sigma$ upper bound (solid red line) and the $2\sigma$ lower bound (dotted red line) produced by this Letter. The shaded areas are disfavored by the constraint on $y_e$ from $(g-2)_e$ [90,91], times the constraints on $y_n$ from neutron optics [92] and neutron scattering experiments [92–95] (yellow), hydrogen and deuterium spectroscopy using electron scattering or the Lamb shift in muonic atoms to determine the charge radius [96] (see also Ref. [97]), fifth force searches [98,99], stellar evolution in the globular cluster [100,101], and energy loss in the supernova SN1987A [102]. The dashed curves show the constraint on $y_e$ from $(g-2)_e$ times the constraint on $y_n$ from $K \to \pi +$ invisible, assuming the new boson $\phi$ couples only to the top-quark (via $y_t$) or only to the up-quark (via $y_u$). The purple band labeled "Be" indicates the coupling range required for a protophobic boson with $m_\phi = 17\ \mathrm{MeV}/c^2$ to explain the ATOMKI anomaly [103].

Our measurements, combined with atomic structure calculations, have enabled a first direct extraction of the evolution of $\delta\langle r^4\rangle$ across the ytterbium isotope chain. To understand whether the change in the nuclear charge distribution is consistent with the strong interaction, we have performed *ab initio* calculations based on chiral effective field theory interactions. Our results reproduce the experimental $\delta\langle r^4\rangle$ remarkably well for such heavy nuclei. The $\langle r^4\rangle$ nuclear charge moment can provide information about both nuclear deformation [6] (because Yb nuclei are prolate deformed) and the surface thickness of the nuclear density [104,105]. It has also been shown that this charge moment can provide insights to experimentally estimate the neutron-skin thickness [105,106]. An exciting future direction is to advance this Letter to the neutron-rich calcium isotopes. This can widen the search for the new boson and shed light on the puzzling increase of charge radii towards $^{52}$Ca [2].

Our isotope-shift and nuclear mass measurements, combined with the isotope-shift measurements of Ref. [80] allow us to set competitive spectroscopy bounds on new bosonic mediators between neutrons and electrons using the generalized King-plot method [11]. With increasing experimental precision, data from more isotopes will be needed to overcome atomic and nuclear structure uncertainties. In ytterbium, a possible candidate is $^{166}$Yb, with a half-life of 54 h. Another option is to use elements Sn [107] or Xe [108], each with seven spinless, stable isotopes and suitable clock transitions that could be found in different ionization stages [109].

*Acknowledgments*—We thank the referees for very valuable feedback on the manuscript. We thank Joonseok Hur, Martin Steinel, and Vladan Vuletić for helpful discussions. This work is supported by the Max Planck Society (MPG), the International Max Planck Research Schools for Precision Tests of Fundamental Symmetries (IMPRS-PTFS), the European Research Council (ERC) under the European Union's Horizon 2020 research and innovation programme under Grant Agreements No. 832848 (FunI) and No. 101020842 (EUSTRONG), and by the Deutsche Forschungsgemeinschaft (DFG, German Research Foundation)—Project-ID 273811115—SFB 1225 ISOQUANT as well as under Germany's Excellence Strategy—EXC-2123 QuantumFrontiers—390837967 (RU B06) and through Grant No. CRC 1227 (DQ-*mat*, projects B02 and B03). This work has been supported by the Max-Planck-RIKEN-PTB-Center for Time, Constants, and Fundamental Symmetries. L. S. D. acknowledges support from the Alexander von Humboldt Foundation. This work comprises parts of the Ph.D. thesis work of M. D. submitted to Heidelberg University, Germany, parts of the Ph.D. thesis work of C.-H. Y. submitted to Leibniz Universität Hannover, Germany, and parts of the Ph.D. thesis work of M. H. submitted to the TU Darmstadt, Germany. M. H., T. M., and A. S. gratefully acknowledge the computing time provided on the high-performance computer Lichtenberg at the NHR Centers NHR4CES at TU Darmstadt and the Gauss Centre for Supercomputing e.V. for funding this project by providing computing time through the John von Neumann Institute for Computing (NIC) on the GCS Supercomputer JUWELS at Jülich Supercomputing Centre (JSC). N. S. acknowledges the support of the "Program for promoting research on the supercomputer Fugaku," MEXT, Japan (JPMXP1020230411), and the MCRP program of the Center for Computational Sciences, University of Tsukuba (NUCLSM). E. F. and F. K. thank CERN for their hospitality during the early phase of this work.

[1] M. S. Safronova *et al.*, Rev. Mod. Phys. **90**, 025008 (2018).
[2] R. F. Garcia Ruiz *et al.*, Nat. Phys. **12**, 594 (2016).

[3] C. Delaunay *et al.*, Phys. Rev. D **96**, 093001 (2017).
[4] J. C. Berengut *et al.*, Phys. Rev. Lett. **120**, 091801 (2018).
[5] I. Counts *et al.*, Phys. Rev. Lett. **125**, 123002 (2020).
[6] S. O. Allehabi *et al.*, Phys. Rev. A **103**, L030801 (2021).
[7] J. Hur *et al.*, Phys. Rev. Lett. **128**, 163201 (2022).
[8] D. A. Nesterenko *et al.*, Int. J. Mass Spectrom. **458**, 116435 (2020).
[9] R. Rana, M. Höcker, and E. G. Myers, Phys. Rev. A **86**, 050502(R) (2012).
[10] J. Repp *et al.*, Appl. Phys. B **107**, 983 (2012).
[11] J. C. Berengut *et al.*, Phys. Rev. Res. **2**, 043444 (2020).
[12] H. Hergert *et al.*, Phys. Rep. **621**, 165 (2016).
[13] S. R. Stroberg *et al.*, Annu. Rev. Nucl. Part. Sci. **69**, 307 (2019).
[14] H. Hergert, Front. Phys. **8**, 379 (2020).
[15] T. Miyagi *et al.*, Phys. Rev. C **105**, 014302 (2022).
[16] E. Epelbaum, H. W. Hammer, and U. G. Meißner, Rev. Mod. Phys. **81**, 1773 (2009).
[17] W. H. King, J. Opt. Soc. Am. **53**, 638 (1963).
[18] C. Roux *et al.*, Appl. Phys. B **107**, 997 (2012).
[19] A. Rischka *et al.*, Phys. Rev. Lett. **124**, 113001 (2020).
[20] L. S. Brown and G. Gabrielse, Phys. Rev. A **25**, 2423 (1982).
[21] C. Froese Fischer *et al.*, Comput. Phys. Commun. **237**, 184 (2019).
[22] W. J. Huang *et al.*, Chin. Phys. C **45**, 030002 (2021).
[23] E. Tiesinga *et al.*, Rev. Mod. Phys. **93**, 025010 (2021).
[24] K. Pyka *et al.*, Appl. Phys. B **114**, 231 (2014).
[25] J. Keller *et al.*, Phys. Rev. Appl. **11**, 011002 (2019).
[26] D. G. Matei *et al.*, Phys. Rev. Lett. **118**, 263202 (2017).
[27] R. Lange *et al.*, Phys. Rev. Lett. **126**, 011102 (2021).
[28] See Supplemental Material at http://link.aps.org/supplemental/10.1103/PhysRevLett.134.063002 for details on the experimental procedures and systematic effects as well as details on the models and methods used for the data analysis and calculations, which includes Refs. [29–79].
[29] R. X. Schüssler *et al.*, Nature (London) **581**, 42 (2020).
[30] P. Filianin *et al.*, Phys. Rev. Lett. **127**, 072502 (2021).
[31] K. Kromer *et al.*, Eur. Phys. J. A **58**, 202 (2022).
[32] K. Kromer *et al.*, Phys. Rev. C **109**, L021301 (2024).
[33] C. Schweiger *et al.*, Rev. Sci. Instrum. **90**, 123201 (2019).
[34] N. E. Bradbury and R. A. Nielsen, Phys. Rev. **49**, 388 (1936).
[35] E. A. Cornell *et al.*, Phys. Rev. A **41**, 312 (1990).
[36] D. J. Wineland and H. G. Dehmelt, J. Appl. Phys. **46**, 919 (1975).
[37] E. A. Cornell *et al.*, Phys. Rev. Lett. **63**, 1674 (1989).
[38] L. S. Brown and G. Gabrielse, Rev. Mod. Phys. **58**, 233 (1986).
[39] J. Ketter *et al.*, Int. J. Mass Spectrom. **358**, 1 (2014).
[40] R. S. Van Dyck *et al.*, Phys. Rev. A **40**, 6308 (1989).
[41] M. Schuh *et al.*, Phys. Rev. A **100**, 023411 (2019).
[42] S. Rau *et al.*, Nature (London) **585**, 43 (2020).
[43] A. Kramida, Y. Ralchenko, J. Reader, and NIST ASD Team, NIST Atomic Spectra Database (version 5.11), Online (2023).
[44] I. P. Grant, Adv. Phys. **19**, 747 (1970).
[45] J. P. Desclaux, D. F. Mayers, and F. O'Brien, J. Phys. B **4**, 631 (1971).
[46] I. P. Grant, *Relativistic Quantum Theory of Atoms and Molecules: Theory and Computation* (Springer, New York, 2007).
[47] P. Jönsson *et al.*, Atoms **11**, 7 (2023).
[48] A. V. Malyshev *et al.*, Phys. Rev. A **90**, 062517 (2014).
[49] A. V. Malyshev *et al.*, Phys. Rev. Lett. **126**, 183001 (2021).
[50] P. Jönsson *et al.*, Atoms **11**, 68 (2023).
[51] C. Lyu *et al.*, Mol. Phys. **0**, e2252105 (2023).
[52] Bureau International des Poids et Mesures (BIPM), https://www.bipm.org/documents/20126/69375142/171Yb+_642THz_2021.pdf/a22c77ad-0c15-e054-ee6c-b7114a23a7a3 (2022).
[53] E. C. Beaty, J. Appl. Phys. **61**, 2118 (1987).
[54] J. Keller *et al.*, Appl. Phys. B **116**, 203 (2014).
[55] H. A. Fürst *et al.*, Phys. Rev. Lett. **125**, 163001 (2020).
[56] C.-H. Yeh *et al.*, New J. Phys. **25**, 093054 (2023).
[57] C. F. Roos *et al.*, Nature (London) **443**, 316 (2006).
[58] T. R. Tan *et al.*, Phys. Rev. A **104**, L010802 (2021).
[59] R. Lange *et al.*, Phys. Rev. Lett. **125**, 143201 (2020).
[60] J. Keller *et al.*, J. Appl. Phys. **118**, 104501 (2015).
[61] N. Huntemann *et al.*, Phys. Rev. Lett. **116**, 063001 (2016).
[62] E. Peik, T. Schneider, and C. Tamm, J. Phys. B **39**, 145 (2005).
[63] T. Lindvall *et al.*, Metrologia **60**, 045008 (2023).
[64] C. Sanner *et al.*, Nature (London) **567**, 204 (2019).
[65] K. Tsukiyama, S. K. Bogner, and A. Schwenk, Phys. Rev. Lett. **106**, 222502 (2011).
[66] D. R. Entem and R. Machleidt, Phys. Rev. C **68**, 041001 (R) (2003).
[67] J. Simonis *et al.*, Phys. Rev. C **96**, 014303 (2017).
[68] S. R. Stroberg *et al.*, Phys. Rev. Lett. **126**, 022501 (2021).
[69] K. Hebeler, Phys. Rep. **890**, 1 (2021).
[70] P. Arthuis, K. Hebeler, and A. Schwenk, arXiv:2401.06675.
[71] A. Ong, J. C. Berengut, and V. V. Flambaum, Phys. Rev. C **82**, 014320 (2010).
[72] J. L. Friar, J. Martorell, and D. W. L. Sprung, Phys. Rev. A **56**, 4579 (1997).
[73] P. Bogdanovich and G. Žukauskas, Sov. Phys. Collect. **23**, 13 (1983).
[74] M. G. Kozlov, S. G. Porsev, and V. V. Flambaum, J. Phys. B **29**, 689 (1996).
[75] M. G. Kozlov *et al.*, Phys. Rev. A **105**, 052805 (2022).
[76] C. Delaunay *et al.*, Phys. Rev. D **96**, 115002 (2017).
[77] M. P. A. Jones, R. M. Potvliege, and M. Spannowsky, Phys. Rev. Res. **2**, 013244 (2020).
[78] K. Blum and D. Kushnir, Astrophys. J. **828**, 31 (2016).
[79] S. Knapen, T. Lin, and K. M. Zurek, Phys. Rev. D **96**, 115021 (2017).
[80] K. Ono *et al.*, Phys. Rev. X **12**, 021033 (2022).
[81] N. L. Figueroa *et al.*, Phys. Rev. Lett. **128**, 073001 (2022).
[82] I. Angeli and K. P. Marinova, At. Data Nucl. Data Tables **99**, 69 (2013).
[83] N. Shimizu *et al.*, Phys. Rev. C **103**, 014312 (2021).
[84] K. Hebeler *et al.*, Phys. Rev. C **83**, 031301(R) (2011).
[85] W. G. Jiang *et al.*, Phys. Rev. C **102**, 054301 (2020).
[86] M. Heinz *et al.*, Phys. Rev. C **103**, 044318 (2021).
[87] E. V. Kahl and J. C. Berengut, Comput. Phys. Commun. **238**, 232 (2019).
[88] C. Solaro *et al.*, Phys. Rev. Lett. **125**, 123003 (2020).
[89] T. T. Chang *et al.*, Phys. Rev. A **110**, L030801 (2024).

[90] D. Hanneke, S. Fogwell, and G. Gabrielse, Phys. Rev. Lett. **100**, 120801 (2008).
[91] X. Fan *et al.*, Phys. Rev. Lett. **130**, 071801 (2023).
[92] H. Leeb and J. Schmiedmayer, Phys. Rev. Lett. **68**, 1472 (1992).
[93] V. V. Nesvizhevsky, G. Pignol, and K. V. Protasov, Phys. Rev. D **77**, 034020 (2008).
[94] Y. N. Pokotilovski, Phys. At. Nucl. **69**, 924 (2006).
[95] R. Barbieri and T. E. O. Ericson, Phys. Lett. **57B**, 270 (1975).
[96] C. Frugiuele *et al.*, Phys. Rev. D **96**, 015011 (2017).
[97] R. M. Potvliege, A. Nicolson, M. P. A. Jones, and M. Spannowsky, Phys. Rev. A **108**, 052825 (2023).
[98] M. Bordag, U. Mohideen, and V. M. Mostepanenko, Phys. Rep. **353**, 1 (2001).
[99] M. Bordag *et al.*, *Advances in the Casimir Effect* (Oxford University Press, Oxford, 2009).
[100] J. A. Grifols and E. Masso, Phys. Lett. B **173**, 237 (1986).
[101] J. A. Grifols, E. Masso, and S. Peris, Mod. Phys. Lett. A **04**, 311 (1989).
[102] G. Raffelt, Phys. Rev. D **86**, 015001 (2012).
[103] A. J. Krasznahorkay *et al.*, Phys. Rev. Lett. **116**, 042501 (2016).
[104] P.-G. Reinhard, W. Nazarewicz, and R. F. Garcia Ruiz, Phys. Rev. C **101**, 021301(R) (2020).
[105] H. Kurasawa, T. Suda, and T. Suzuki, Prog. Theor. Exp. Phys. **2021**, 013D02 (2021).
[106] T. Naito, G. Colò, H. Liang, and X. Roca-Maza, Phys. Rev. C **104**, 024316 (2021).
[107] D. R. Leibrandt, S. G. Porsev, C. Cheung, and M. S. Safronova, Nat. Commun. **15** (2024).
[108] N.-H. Rehbehn *et al.*, Phys. Rev. Lett. **131**, 161803 (2023).
[109] C. Lyu, C. H. Keitel, and Z. Harman, Commun. Phys. **8**, 3 (2025).
[110] F. Heiße *et al.*, Phys. Rev. Lett. **119**, 033001 (2017).

## End Matter

*Probing new bosons and nuclear structure with ytterbium isotope shifts*—In Fig. 3 we present an overview over the two experimental setups as well as a King plot of the isotope shifts of the $\gamma$ transition with respect to the isotope shifts of the $\alpha$ transition normalized with the inverse mass-ratio difference $w^{A,A'}$.

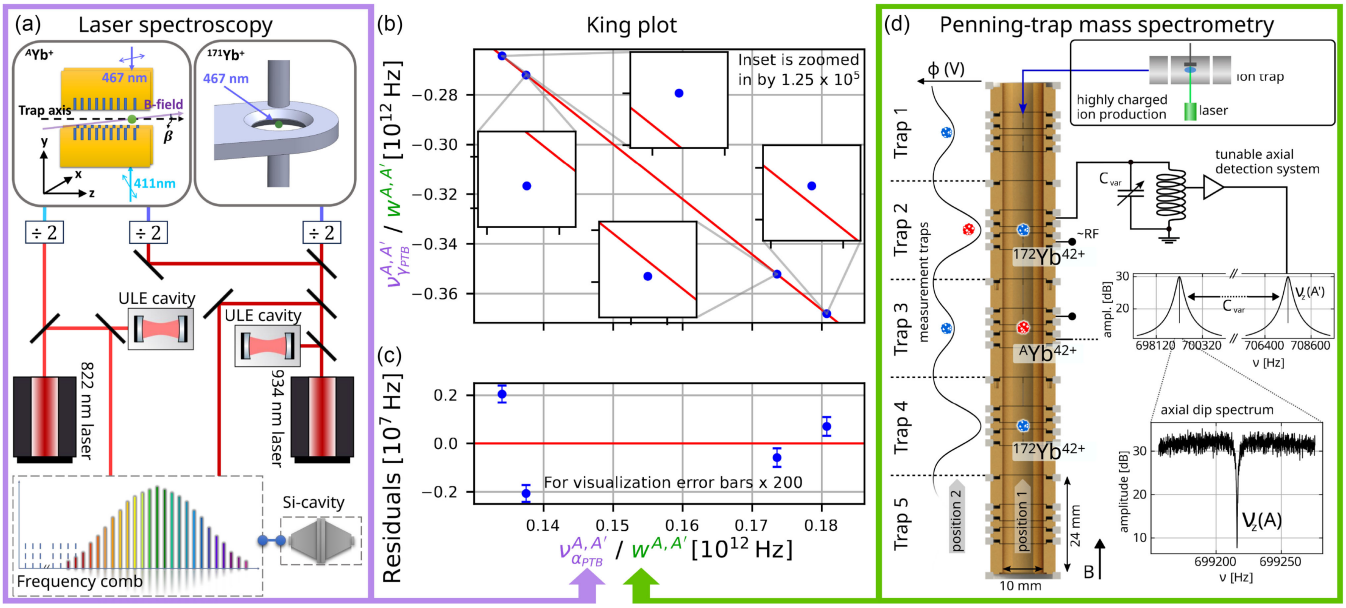


FIG. 3. Scheme of experimental setups and the King-plot analysis. (a) Laser spectroscopy setup for the optical frequency ratio measurements of the transitions near 411 ($\alpha$) and 467 nm ($\gamma$). The laser fields with wavelengths near 822 and 934 nm are first stabilized to an ultra-low expansion (ULE) cavity for short-term frequency stability and then locked to a cryogenic silicon cavity (Si cavity). The second harmonic conversions of the lasers are focused to interrogate the ions. (b) King plot of the isotope shifts of the $\gamma$ transition with respect to the isotope shifts of the $\alpha$ transition normalized with the inverse mass-ratio difference $w^{A,A'}$, with insets magnified by a factor of $1.25 \times 10^5$. (c) Residuals of the linear fit in the King plot. For visibility, the uncertainties on the residuals are multiplied by a factor of 200. (d) Penning-trap setup for the determination of cyclotron frequency ratios. Three highly charged ions (blue and red), produced by an electron beam ion trap, are transported and stored in an $A'$-$A$-$A'$ sequence. By shuttling the set of ions up and down between neighboring traps (alternating between positions 1 and 2), cyclotron frequency ratios are determined from sequential measurements in the two measurement traps, referred to trap 2 and 3 in the figure. The tunable image-current detection system allows for the determination of the axial eigenfrequencies of different isotopes at equal charge state and equal trapping potential [110]. The radial eigenfrequencies are determined indirectly using the same detection system.